Modelling thermodynamics in a high-temperature superconducting dipole magnet: an inverse problem based approach

J Ruuskanen[1], A Stenvall[1], V Lahtinen[1], J van Nugteren[2], G Kirby[2] and J Murtomäki[1]

[1] Tampere University, Korkeakoulunkatu 6, FI-33101 Tampere, Finland
[2] CERN, CH-1211 Geneva 23, Geneva, Switzerland

E-mail: janne.ruuskanen@tuni.fi

30 November 2020

Abstract. The use of practical high temperature superconductors (HTS), REBCO tapes especially, in magnet applications has become possible thanks to the increasing interest of manufacturers. One difficulty has been the non-linear material properties that are challenging to measure and model. To advance in such, demo systems are needed and they must be thoroughly analyzed. Recently, one of the first HTS dipole magnets was built to study the usability of REBCO Roebel cables in particle accelerator magnets. The prototype magnet Feather-M2 was designed, constructed and tested within EUCARD2 collaboration project at CERN in 2017. In the measurements, the magnet behaved in an unexpected way: the magnet was able to be operated at operation currents above the maximum current that was predicted based on short-sample measurements. Additionally, unexpectedly gradual dependency between magnet's resistive voltage and operation current was observed. In this work, a thermodynamical model is formulated in order to study the behavior of Feather-M2. The model was parametrized and the parameters were solved via inverse problem by finding the best match to experimental results. Thereby insight was gained on the prospects of the utilized thermodynamical model and also on the behavior and operation conditions of the magnet via the inverse problem solutions. To summarize, this paper presents a new methodology for analyzing magnets in operation and applies it to a state-of-the-art magnet.

Keywords: HTS magnets, modelling, optimization, stability

Submitted to: *Supercond. Sci. Technol.*

1. Introduction

High electric current carrying capability of practical high-temperature superconductors (HTS) has been a tempting property to harness into use in applications [1, 2, 3]. The main problem in the design process of HTS based devices arises from the highly nonlinear material properties that are challenging to measure and model. Recently, however, the suitability of using high temperature superconductors in particle accelerator dipole-magnets was experimentally investigated: a REBCO Roebel cable [4] based prototype magnet, Feather-M2, was designed, constructed and tested within EUCARD2 [5] collaboration project at CERN [6] in 2017. The specifications in regards of the magnet, measurement set-up and the results were presented in [7].

The measurements revealed magnet behavior not yet in detail analyzed within the HTS community – the magnet could be operated above its critical current (I_c) without quench, where I_c was defined using electric field criterion of 10 μV/m. In other words, it was not possible to predict the quench current based on the short sample measurements. This is different behavior from what is expected for low-temperature superconductor (LTS) based magnets since the quench current of an LTS magnet is limited above by the short-sample I_c. However, the observed unpredicted behavior needed to be investigated and explained.

To study the observed behavior, the heat equation can be solved in the modelling domain representing the magnet under investigation. Research on the thermal modelling of HTS magnets has been done by many authors, e.g., [8, 9, 10, 11, 12, 13]. Typically the focus has been on investigating the fast during- and after-quench effects such that the use of adiabatic boundary conditions (cooling is neglected) could have been justified. Typically this kind of modelling is related to the quench simulations in which the focus is mainly on magnet protectability in the occurrence of thermal runaway. However, in order to simulate situation in which the magnet is operated with relatively high currents for long periods of time, the cooling should be taken into account in the modelling as done and discussed in [14, 15, 16] to name some.

Modelling thermodynamics in a superconducting magnet is a multiphysical problem. When formulating the problem using different models, the values of some model parameters may be unknown, such as, the value for the heat transfer coefficient in the model describing the cooling at the boundary of the winding. Values for such model parameters can be hard to find from literature for a particular case. However, if there exists measured data on the phenomenon one is trying to model, it can be used to solve unknown model parameters. Such problems, in which based on results known beforehand one calculates the causes, are called inverse problems.

An inverse problem can be solved in various different ways depending on their nature. One way of obtaining a solution for such a problem is to reformulate it as an optimization problem and solve it using optimization algorithms. For example in [17], the Kim model used to describe the critical electric current density in REBCO superconducting material was parametrized and the parameters were obtained as a solution of an optimization problem based on measured data. In the field of astronomy and astrophysics, recently, the parameters of the equation of state of the cold dense matter inside neutron stars based on X-ray measurements [18] were determined by solving an Bayesian parameter optimization problem. In [19], magnet cross-section was parametrized and optimized based on minimum cost criterion.

This paper focuses on modelling thermodynamics in an HTS magnet and studying its thermal stability in operation. In this work, a thermodynamical model is formulated in order to model the thermal behavior of an HTS magnet. The aim is to improve our understanding on the magnet behavior and on the other hand, gain insight on the capability of the implemented modelling tool in predicting the thermodynamics in the magnet. In order to do so, the model is parametrized and the parameters are obtained based on measured data on the HTS magnet Feather-M2 by means of formulating and solving an inverse problem.

The paper is outlined as follows. Section 2 continues the introductory part of the paper by reviewing the essential information on the measurements of Feather-M2 for this work. In section 3 and section 4, the methodology utilized in this work is presented. Section 3 concentrates on the multiphysical model of the magnet and section 4 on solving via inverse problem the unknown parameters. In section 5, the simulation results are shown with appropriate discussion. Finally conclusions are drawn in section 6.

Table 1. Magnet specifications, as used in the modelling.

dimension	value	unit
number of turns (wing deck)	4	
number of turns (central deck)	8	
total cable length	37	m
total tape length	555	m
magnet length	720	mm
peak field (6.5 kA, 5.7 K)	3.3	T

Table 2. Roebel-cable specifications, as used in the modelling.

dimension	value	unit
number of tapes	15	
cable width	12.0	mm
cable thickness	1.2	mm
cable insulation thickness (G10)	0.1	mm

Table 3. Tape specifications, as used in the modelling,

dimension	value	unit
tape width	5.5	mm
tape thickness	150	μm
Ag	1	μm
Cu	40	μm
REBCO	1.4	μm
Hastelloy	100	μm
buffer	7.6	μm

2. Measured data on HTS magnet Feather-M2

Feather-M2, a Roebel cable based accelerator magnet prototype, studied in this work, is one of the first magnets of its type built and tested. In this section, the physical system, consisting of the magnet and the cooling environment, are presented to sufficient detail. In addition, the measurement data, adequate for this work, is shown. The original work regarding to the measurement results was presented in [7].

2.1. Feather-M2

A representation of Feather-M2 is shown in figure 1 and the magnet specifications are listed in table 1. The magnet has two poles, named as Feather-M2.1 and Feather-M2.2. Both of them consists of two race track shape coils – a larger central deck and a smaller wing deck. The central deck has 8 turns of Roebel cable and the wing deck has 4 turns. The total length of Roebel cable required for the 0.7 meters long magnet was 37 meters, i.e., 18.5 meters per pole. It was reported that the maximum achieved magnetic field in the magnet aperture was 3.3 T, at 5.7 K, at the current of 6.5 kA [7].

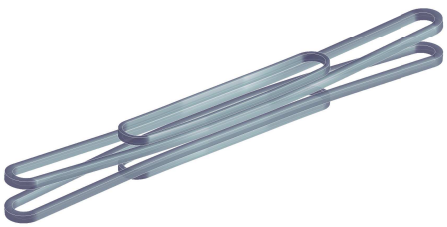

Figure 1. Depiction of the dipole magnet Feather-M2. Figure adapted from [20].

The Roebel cable was made by SuperOx [21]. The REBCO tapes utilized in making the cable were manufactured by Sunam [22]. The cable specifications are listed in table 2 and the specifications related to the tape, as used in the modelling, are listed in table 3. The cable consists of 15 tapes that are cabled into Roebel form (see [7]). This results in cable cross-sectional dimensions of 1.2 mm $\times$ 12.0 mm. In addition, the cable was insulated with 0.1 mm thick G10 fiber glass, functioning as electric insulation. Hence, the cable's total thickness d_{t} is 1.4 mm and the total width d_{w} is 12.2 mm. Between two cable turns, the total insulation thickness d_{i} is 0.2 mm. Each of the tapes in the cable has cross-sectional dimensions of 150 μm $\times$ 5.5 mm, and consists of several different material layers as listed in table 3. Total tape length is 555 m.

2.2. Measurements

The magnet, under investigation in this work, was tested at CERN in SM18 facility [23]. Cooling was realized in a cryostat using forced helium gas flow with adjustable flow rate and temperature. The measurement data shown in figure 2 represents the resistive average electric field over the Feather-M2.1 pole, as a function of operation current I_{op} and time. The average electric field is calculated as the resistive voltage over the pole divided by the cable length. For simplicity, in this paper, we assume the two poles are identical in behavior. Therefore, it is sufficient in the thermal computations to investigate only one of the two magnet poles. Moreover, magnet's operation temperature T_{op} was measured using temperature sensors mounted inside the magnet structure.

The measurement data in figure 2 shows magnet behavior in various temperatures with different operation currents varying in time. In this work, using this data we will investigate how well the thermodynamical model, next formulated, is capable of predicting the thermodynamical behavior of the magnet.

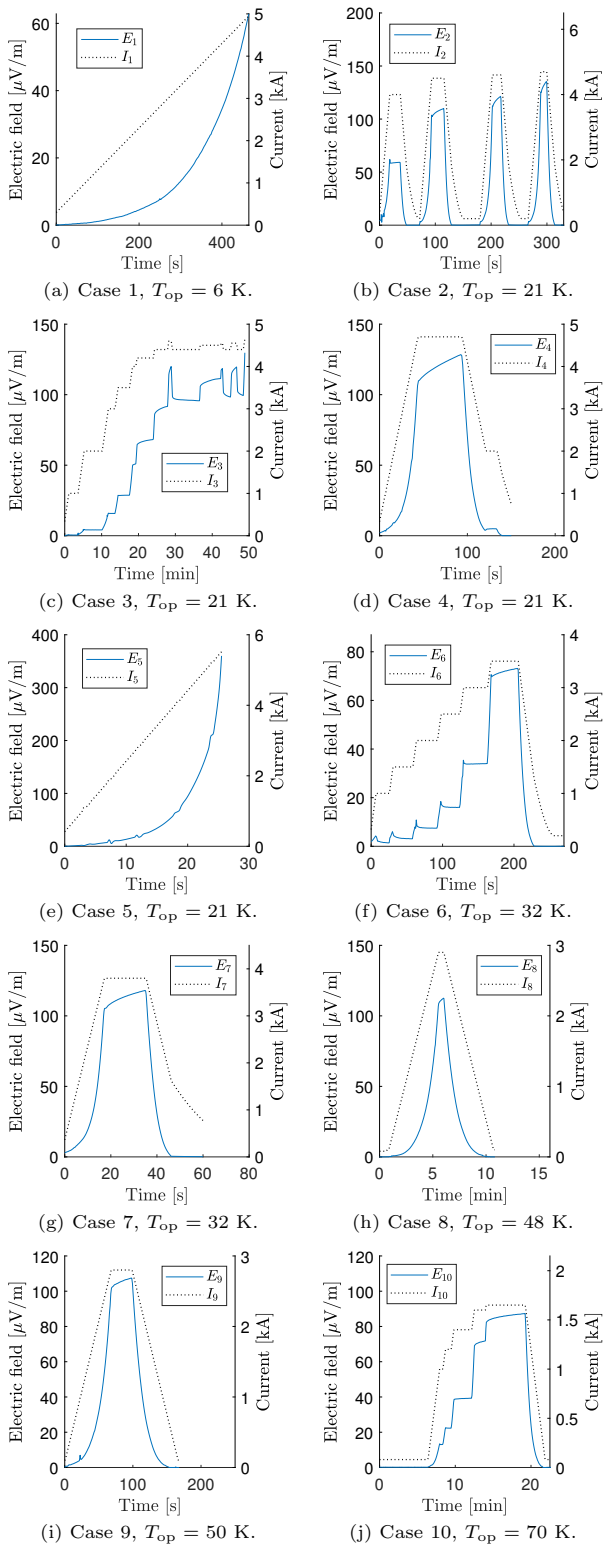

(a) Case 1, $T_{\text{op}} = 6$ K. (b) Case 2, $T_{\text{op}} = 21$ K.

(c) Case 3, $T_{\text{op}} = 21$ K. (d) Case 4, $T_{\text{op}} = 21$ K.

(e) Case 5, $T_{\text{op}} = 21$ K. (f) Case 6, $T_{\text{op}} = 32$ K.

(g) Case 7, $T_{\text{op}} = 32$ K. (h) Case 8, $T_{\text{op}} = 48$ K.

(i) Case 9, $T_{\text{op}} = 50$ K. (j) Case 10, $T_{\text{op}} = 70$ K.

Figure 2. Figures (a)-(j) represent, in each case $i = 1...10$, the measured average electric field E_i as a function of the operation current I_i and time in Feather-M2.

3. A thermodynamical model for HTS magnet

In this section, a model for predicting thermodynamics in HTS magnets is formulated. In this work the formulation of the model is based on the heat diffusion equation

$$C_{\text{V}} \frac{\mathrm{d}}{\mathrm{d}t} T = \frac{\mathrm{d}}{\mathrm{d}x} \left(\lambda \frac{\mathrm{d}}{\mathrm{d}x} T \right) + Q^{+} + Q^{-} + Q^{\parallel}, \tag{1}$$

where T, λ are the temperature and the thermal conductivity, respectively. The terms C_{V}, Q^{+}, Q^{-} and $Q^{\parallel}$ represent the volumetric heat capacity, the heat generation, the cooling and the heat transfer between the cable turns, respectively.

We omit the magnetoquasistatic phenomena and assume constant electric current density in the cable's normal- and superconducting cross-sectional fraction. Furthermore, homogeneous temperature in the cable cross-section is assumed. Therefore, the temperature in the cable, and hence in the magnet, can be modelled in 1-dimensional modelling domain. In addition, heat exchange between the cable turns is taken into account as source term describing the heat flux between the turns due to temperature difference in adjacent turns.

This section goes through the constructive framework for performing thermal simulations in a superconducting magnet by formulating the terms of (1). In addition, a discretization method is presented for numerical solution of the heat equation in coil shaped domains.

3.1. Domain and discretization

When solving for continuous field quantities in 3-dimensional (3-D) geometries, such as electromagnetic fields in coils, the fine details in the geometry require a fine mesh resulting in a large number of degrees of freedoms. However, in some cases, fine meshing can be avoided by choices on the dimension of the modelling domain and its discretization, as done in this work.

In this simulation approach, the modelling decision on homogeneous temperature in the cable cross-section is deployed [10]. Therefore, the heat transfer along the cable can be modelled utilizing 1-dimensional (1-D) modelling domain, which in this work was discretized using the Galerkin finite element method with linear basis functions.

The 3-D to 1-D reduction in dimension can be illustrated by first having a look at figure 3, where a part of a coil, a piece of two adjacent insulated cable turns, is depicted. After homogenizing the cable cross-section, a coil can be illustrated as a spiral shown in figure 4, where the cable progression and adjacency is visualized. To emphasize, even though we have formulated our model for 1-D modelling domain, we still utilize the cable-to-cable heat conduction as will be shown.

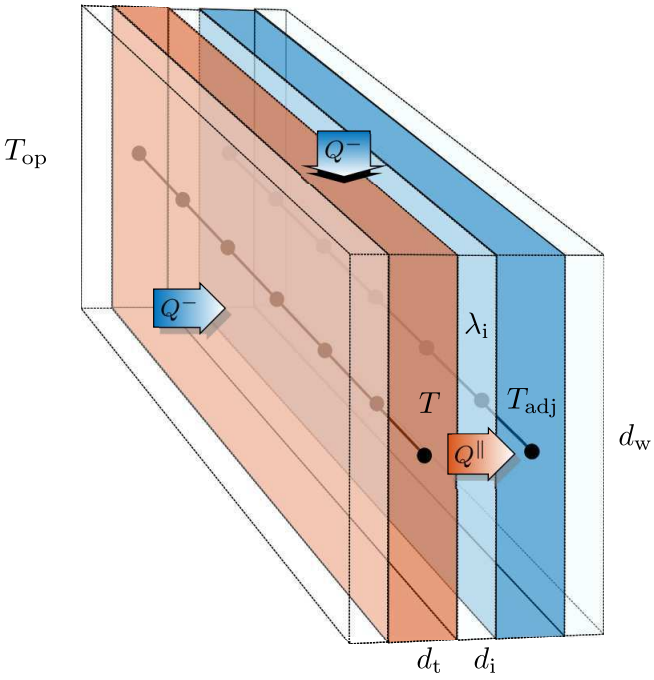

Figure 3. An illustration of a piece of two adjacent insulated cable turns. Figure illustrates the different heat flux terms, i.e., the one from turn to another ($Q^{\parallel}$), and also the cooling flux (Q^-) on the exposed surfaces of the winding. Cable insulation is visible only in between the cable turns.

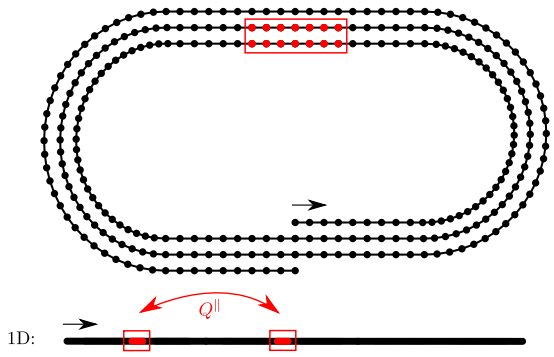

Figure 4. A visualization of the progression and adjacency of the homogenized cable. The coil piece shown in figure 3 is marked as the boxed regions.

3.2. Material properties

Due to modelling decision on dimension reduction to 1-D, the properties, C_{V}, λ and ρ_{nc} must be homogenized over the cable cross-section [24].

The formulae for computing the material properties of homogenized materials are the following three.

$$C_{\mathrm{V}} = \sum_{i=1}^{m} f_i \cdot C_{\mathrm{V}}^i \tag{2}$$

$$\lambda = \sum_{i=1}^{m} f_i \cdot \lambda^i \tag{3}$$

$$\rho_{\mathrm{nc}} = \left(\sum_{i=1}^{n} \frac{g_i}{\rho_{\mathrm{nc}}^i} \right)^{-1} \tag{4}$$

In equations (2) and (3), m refers to the number of different materials in the cable, including the superconducting material, such that $\sum_{i=1}^{m} f_i = 1$, where f_i is the fraction of material i. Equation (4) describes the resistivity of the homogenized normal conducting materials of the cable, where superconducting material is not involved, i.e., $\sum_{i=1}^{n} g_i = 1$ where $n = m - 1$ is the number of normal conducting materials, including the insulators which naturally have very high resistivity, in the cable and g_i is the fraction of material i in the cross-sectional area of normal conducting materials.

3.3. Critical current

Critical current is a quantity used to describe the $E_{\mathrm{sc}}(I_{\mathrm{sc}})$ relation, i.e. the power law (6), in the superconducting material of the cable together with the electric field criterion and the n-value. On its own, it is a somewhat arbitrary quantity for superconductors with low n-value due to gradual dependency. It is, however, necessary data on the superconductor's behavior that is utilized in the power law model.

The measurement data on superconductor's I_{c} properties is typically obtained and performed for single superconducting wires, short samples. A single I_{c} measurement point is determined in certain cooling conditions and temperature by increasing sample's current until the voltage reaches arbitrarily selected value – the critical voltage (V_c). For modelling purposes, the obtained values for critical voltage criterion V_{c} and critical current are often scaled to critical field quantities critical current density J_{c} and critical electric field E_{c}. Using this data, interpolating function J_{c} is fitted to match the measured data. In addition to temperature, magnetic field is one variable in the measurements and thus in the J_{c} function. In the case of REBCO tapes, wide compared to their thickness, the direction of the magnetic field has a significant influence on J_{c}.

In this work, we take a measurement based J_{c} scaling law and commence formulating a computational model for I_{c} in the superconducting material used in the magnet.

As the modelling domain in the approach utilized in this work is 1-dimensional, we are interested in the local cross-sectional critical current along the length of the cable in the magnet. It is computed by integrating J_{c} over the superconducting parts of the cable cross-

section as

$$I_{\mathrm{c}}(T, I_{\mathrm{op}}, \alpha) = \int_{A_{\mathrm{sc}}} \alpha J_{\mathrm{c}}(T, \hat{\mathbf{B}} I_{\mathrm{op}}) \, \mathrm{d}A, \tag{5}$$

where $\hat{\mathbf{B}}$ is pre-computed local magnetic flux density per unit current in the 3-dimensional magnet geometry. Note that the function parameters are denoted here for clarification. Furthermore, linear $\mathbf{B}(I_{\mathrm{op}})$ depency is assumed, where I_{op} is the operation current of the magnet. The scaling coefficient α is utilized to scale a J_{c} scaling law to describe the J_{c} characteristics of the utilized superconductor in the application to be modelled. Furthermore, this I_{c} is needed for computing the local cross-sectional electric field and eventually for computing the local heat generation in the modelling domain.

3.4. Heat generation

In superconducting wire, losses can be generated in both, the superconducting fraction (f_{sc}) and in the normal conducting fraction (f_{nc}) of the conductor. Due to significantly different $E(J)$ behavior in f_{sc} and f_{nc}, the heat generation in the two fractions is modelled separately by solving the electric current division based on the $E - J$ characteristics in the two fractions.

In the superconducting material the electric field is modelled using the power law

$$E_{\mathrm{sc}} = E_{\mathrm{c}} \left(\frac{I_{\mathrm{sc}}}{I_{\mathrm{c}}} \right)^n, \tag{6}$$

where E_{c} is the electric field criterion and n the n-value that characterizes the steepness of the relation. The electric current I_{sc} is the current flowing in the f_{sc} with constant density of J_{sc}. Hence, the heat generation in f_{sc} is computed as $E_{\mathrm{sc}} J_{\mathrm{sc}} = E_{\mathrm{sc}} I_{\mathrm{sc}} / A_{\mathrm{sc}}$, where A_{sc} is the area of superconducting material in the cross-section of the cable (A). In the normal conducting fraction, E_{nc} due to the electric current density $J_{\mathrm{nc}} = I_{\mathrm{nc}} / A_{\mathrm{nc}}$ is modelled according to the Ohm's law as $E_{\mathrm{nc}} = \rho_{\mathrm{nc}} J_{\mathrm{nc}}$, where ρ_{nc} is the effective resistivity of the homogenized materials of f_{nc} having cross-sectional area of $A_{\mathrm{nc}} = f_{\mathrm{nc}} A$.

The total current, i.e. the operation current (I_{op}), is assumed to divide between the two fractions into I_{sc} and I_{nc} such that $E_{\mathrm{sc}} = E_{\mathrm{nc}}$ and $I_{\mathrm{op}} = I_{\mathrm{sc}} + I_{\mathrm{nc}}$ hold. Consequently the current in the normal conducting part of the cross-section, can be derived as follows.

$$\begin{aligned}
& E_{\mathrm{nc}} && = E_{\mathrm{sc}} \\
\Leftrightarrow\ & \rho_{\mathrm{nc}} \frac{I_{\mathrm{nc}}}{A_{\mathrm{nc}}} && = E_{\mathrm{c}} \left(\frac{I_{\mathrm{sc}}}{I_{\mathrm{c}}} \right)^n \\
\Leftrightarrow\ & I_{\mathrm{nc}} && = E_{\mathrm{c}} \left(\frac{I_{\mathrm{sc}}}{I_{\mathrm{c}}} \right)^n \frac{A_{\mathrm{nc}}}{\rho_{\mathrm{nc}}} \\
\Leftrightarrow\ & I_{\mathrm{nc}} && = E_{\mathrm{c}} \left(\frac{I_{\mathrm{op}} - I_{\mathrm{nc}}}{I_{\mathrm{c}}} \right)^n \frac{A_{\mathrm{nc}}}{\rho_{\mathrm{nc}}}
\end{aligned} \tag{7}$$

Hence, the electric current in the normal conducting fraction can be solved from the non-linear equation

$$I_{\mathrm{nc}} - E_{\mathrm{c}} \left(\frac{I_{\mathrm{op}} - I_{\mathrm{nc}}}{I_{\mathrm{c}}} \right)^n \frac{A_{\mathrm{nc}}}{\rho_{\mathrm{nc}}} = 0 \tag{8}$$

and consequently I_{sc} can be calculated as $I_{\mathrm{sc}} = I_{\mathrm{op}} - I_{\mathrm{nc}}$.

As now the current division in the superconducting and normal conducting fractions is known, the volumetric heat generation Q^+ in the homogenized cable is derived as

$$\begin{aligned}
Q^+ &= f_{\mathrm{sc}} E_{\mathrm{sc}} J_{\mathrm{sc}} + f_{\mathrm{nc}} E_{\mathrm{nc}} J_{\mathrm{nc}} \\
&= f_{\mathrm{sc}} E_{\mathrm{c}} \left(\frac{I_{\mathrm{sc}}}{I_{\mathrm{c}}} \right)^n \frac{I_{\mathrm{sc}}}{A_{\mathrm{sc}}} + f_{\mathrm{nc}} \rho_{\mathrm{nc}} \left(\frac{I_{\mathrm{nc}}}{A_{\mathrm{nc}}} \right)^2 .
\end{aligned} \tag{9}$$

Note that $f_{\mathrm{sc}} + f_{\mathrm{nc}} = 1$ has to hold.

3.5. Cooling

Cooling is necessary to take into account when modelling thermodynamics in HTS magnets, as demonstrated for example in [20].

In this work, local cooling on the cable is taken into account in the computations using

$$Q^- = h \frac{T_{\mathrm{op}} - T}{c}, \tag{10}$$

where the heat flux between the coolant and the surface of the winding is determined by cooling coefficient h and the temperature difference between the cooling environment (T_{op}) and the cable (T). Moreover, the scaling factor c is calculated as

$$c = \frac{A}{p}, \tag{11}$$

where A is the cross-sectional area of the cable and p is the local wetted perimeter‡. The purpose of c is to scale the cooling on the surface of an element to cooling in the volume of the element.

There are many uncertainties related to this cooling model. The largest error comes with the facts that Q^-, in reality, is doubtedly a linear function of T, and h varies also as a function of location on the magnet surface in the cryostat. Moreover, due to various structures covering the winding it is hard to determine, how the wetted perimeter should be chosen for each cable turn. However, in this work, we chose this simple model for cooling in order to investigate its prospects.

3.6. Heat transfer between cable turns

The heat transfer between the cable turns in 1-dimensional modelling domain is modelled as local heat flux similarly as the cooling model. Figure 3 and

‡ For example, if at a given point in the modelling domain, all the faces of cable were exposed to the cooling, then the wetted perimeter would be calculated as $p = 2d_{\mathrm{w}} + 2d_{\mathrm{t}}$.

figure 4 illustrate how two adjacent turns are coupled in the 1-dimensional domain.

The local flux to a cable turn from an adjacent one is expressed as

$$Q^{\parallel} = \lambda_{\mathrm{i}} \frac{T_{\mathrm{adj}} - T}{d_{\mathrm{i}} c}, \tag{12}$$

where T and T_{adj} represent temperatures in two adjacent points in two neighboring cable turns separated by insulation material, having the thickness of d_{i}. The material property of the insulation material λ_{i}, describes the temperature dependent thermal conductivity of the insulation material. The thermal conductivity is evaluated at the average temperature of T and T_{adj}. In this case, in the computation of c, the wetted perimeter is the width of the cable.

4. The inverse problem formulation

Often some parameters related to mathematical theories or models are unknown or difficult to determine for a particular case of interest. This is the case in this work too. For example, the cooling coefficient h in the utilized cooling model (10) is difficult to estimate. The same applies to three other parameters: α, n-value and E_{c}. It is not straightforward to give values for the parameters such that the model is able to predict as well as possible the behavior of the device in various different situations. In this work we formulate and solve an inverse problem in order to obtain the unknown parameters of our thermodynamical model.

The parameters to be solved, as elements of $\mathbf{x}$, are $\mathbf{x} = [\alpha, n, E_{\mathrm{c}}, h]$. Recall, α is the J_{c} scaling coefficient in (5) and h the cooling coefficient of the cooling model (10). Parameters n and E_{c} characterize the $E_{\mathrm{sc}}(J_{\mathrm{sc}})$ relation in (6). The model M, i.e. the thermodynamical model, relates the parameters $\mathbf{x}$ with the observed data on average resistive electric field, computed as measured resistive voltage divided by cable length. We want the model M to predict the measured E of the magnet as well as possible in given operation conditions $(T_{\mathrm{op}}, I_{\mathrm{op}})$. Hence, the inverse problem can be expressed as: Find α, n, E_{c} and h such that

$$E_i = \mathrm{M}(\mathbf{x}, I_i), \tag{13}$$

where I_i represent the operation current as a function of time and E_i is the corresponding measurement data on average electric field. The problem is nonlinear, therefore, (13) has to be reformulated to an optimization problem in order to obtain the best candidate for $\mathbf{x}$ so that $\mathrm{M}(\mathbf{x}, I_{\mathrm{op}})$ is as close as E as possible.

An optimization problem consists of an objective function to be minimized subject to constraints that define the set of feasible solutions. In this work, the objective is to minimize the difference between the measured and simulated average electric field in the time interval $[0,\ t_{\mathrm{m}}]$, where t_{m} corresponds to duration of the measurement which started at $t = 0$ s. For the norm, measuring the difference $E - \mathrm{M}(\mathbf{x}, I_{\mathrm{op}})$, we chose the time integral of the absolute value of difference. Hence, the minimization problem can be formulated as

$$\begin{array}{ll} \min\limits_{\mathbf{x}} & \int_t^{t_{\mathrm{m}}} \left| (E_i - \mathrm{M}(\mathbf{x}_i, I_i))\,(t) \right| \mathrm{d}t \\ \text{s.t.} & \mathbf{b}_{\mathrm{l}} \leq \mathbf{x} \leq \mathbf{b}_{\mathrm{u}} \end{array}, \tag{14}$$

where the vectors $\mathbf{b}_{\mathrm{l}}$ and $\mathbf{b}_{\mathrm{u}}$ are the parameter-wise lower- and upper bounds, respectively. These bounds are used to guide the optimization algorithm. The subscript $i = 1...10$ is the number of the case.

5. Interpreting measured data on Feather-M2

In this section, an implementation of the thermal model, formulated in section 3, is utilized for investigating the thermal behavior of Feather-M2 in various operation conditions. The measurement data on the magnet shown in figure 2 is utilized for obtaining values for the unknown parameters of the thermal model as a solution of an inverse problem (14).

The simulation tool was programmed on top of the *dp* framework [26] using Matlab [25]. *Field* was utilized for creating the magnet geometry and for precomputing the magnetic field in 3-dimensional magnet geometry [27]. For solving the heat diffusion equation, the numerical method presented in [28] was utilized. In solving the inverse problems, the optimization algorithm presented in [29] was utilized.

Next, we formulate the thermal problem and solve the inverse problems in all the measured cases in order to obtain solutions for the model parameters. From all of the solutions, we choose the inverse problem solution $\mathbf{x}$ that resulted in smallest difference between E and $\mathrm{M}(\mathbf{x}, I_{\mathrm{op}})$ as a function of time. Using those parameter values, we benchmark the model against all the measured cases in order to study the predictive capability of the thermal model.

5.1. Problem formulation

The problem is formulated, or instantiated, by fixing the material properties and other known parameters. Starting from the magnet geometry, depicted in figure 1 and specified in table 1, the heat equation (1) is discretized for 1-dimensional modelling domain as explained in section 3. The material properties for computing C_{V} and λ in (1), and the resistivity ρ_{nc} in (9), are obtained from the references listed in table 4, where the electrical resistivity of Silver was calculated from λ using the Wiedemann-Franz law. The REBCO

Table 4. References for the material properties.

material	property	reference
Cu	C_V, λ, ρ	[33]
G10	C_V, λ	[33]
Hastelloy	C_V, λ, ρ	[34]
Ag	C_V	[35]
Ag	λ, ρ	[36]

material, in the sense of C_V and λ, is considered as G10. The material fractions are calculated using the cable and tape specifications listed in table 2 and table 3, respectively. The critical current I_c in (5) is computed using a J_c scaling law fitted to match with measurement data on REBCO tape manufactured by Fujikura [30]. The scaling law is described in [8, p. 246-248]. Moreover, in regards of (10), an assumption on constant temperature outside magnet's winding is deployed.

The wetted perimeter p in the cooling model (10) is determined as follows. Figure 5 shows the Feather-M2 cross-section of the upper magnet pole during operation.§ According to the study [31], during magnet operation, the winding detaches from the pole. Using this result, we choose the wetted perimeter such that the cooling is neglected from the inner wide face of the innermost cable turns, i.e., we assume a vacuum in those spaces. Therefore, the wetted perimeter in the inner turns is $p = 2d_t$. In the outermost turns of the wing and central decks $p = d_w + 2d_t$. In the rest of the turns in between $p = 2d_t$, i.e., cooling flux affects through the narrow faces of cable.

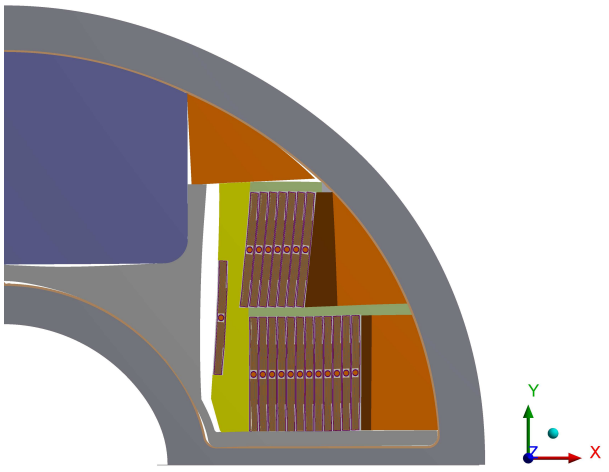

Figure 5. An exaggerated view on the deformation of the magnet's cross-section during its operation. A quarter of magnet's cross-section is shown.

§ In this particular study, a different cable was utilized. Therefore the magnet has more cable turns than in the design investigated in this work.

Table 5. Lower- and upper bounds for the model parameters.

parameter	$\mathbf{b}_l$	$\mathbf{b}_u$	unit
α	0.1	0.3	
n	1	30	
E_c	1	150	μV/m
h	1	300	W/m^{2}K

Furthermore, in solving the inverse problem (14), the lower bounds $\mathbf{b}_l$ and the upper bounds $\mathbf{b}_u$ for the optimization parameters are shown in table 5. Next, the solutions of the inverse problems presented.

5.2. Inverse problem solutions

The inverse problem is solved for each of the measured cases shown in figure 2. The solutions of the model parameters, $\mathbf{x}_i$, are shown in table 6. Figure 6 shows, in each of the cases, the measured average electric field and the prediction of the model, parametrized with the corresponding solution.

The difference between the model predictions and the experimental data is calculated as the relative and maximum difference. The relative difference Δ_r is calculated as

$$\Delta_r = 1 - \frac{\int_0^{t_m} \left(\mathrm{M}(\mathbf{x}, I_{op})\right)(t)\ \mathrm{d}t}{\int_0^{t_m} E(t)\ \mathrm{d}t} \tag{15}$$

and the maximum difference Δ_m as

$$\Delta_m = \max\{|(E - \mathrm{M}(\mathbf{x}, I_{op}))(t)|\},\ t \in [0,\ t_m]. \tag{16}$$

According to the relative differences shown in table 7, the best solution was found in the case 6, where the relative difference was 0.4 % and the maximum difference was 4 μV/m. The solved parameter values in each of the 10 cases are shown in table 6. The parameters that vary the most from case to case are E_c and h while the variance in α and n is smaller.

The results suggest relatively low n-values, i.e., between 2.3 and 3.1. Similar low n-values have also been reported in the original test results of Feather-M2 [7]. The reason for the low n can be related to the J_c (or I_c) variation between the different tapes in the cable [32].

Based on the results, no systematic relation were found between a case and its solution. The reason for this can be that all the cases represent very different operation conditions. Moreover, as the cooling of the magnet was realized with forced flow helium gas, the cooling efficiency can vary significantly in the cryostat. In addition, we had no data on, whether the flow rate of the helium gas was kept the same in all of the measured cases. As for the future analysis of this kind, simpler measurements could be more useful, where the operation current could be ramped up close

Table 6. The solutions of the inverse problems.

	α	n	E_c	h	T_{op}
$\mathbf{x}_1$	0.17	2.3	102	69	6
$\mathbf{x}_2$	0.17	2.8	109	85	21
$\mathbf{x}_3$	0.16	3.1	91	55	21
$\mathbf{x}_4$	0.18	3.0	108	45	21
$\mathbf{x}_5$	0.15	2.9	84	75	21
$\mathbf{x}_6$	0.17	2.9	90	77	32
$\mathbf{x}_7$	0.17	3.3	87	86	32
$\mathbf{x}_8$	0.19	2.8	74	60	48
$\mathbf{x}_9$	0.20	2.5	72	42	50
$\mathbf{x}_{10}$	0.19	3.1	10	44	70
unit			μV/m	W/m^{2}K	K

Table 7. Relative and maximum differences of the inverse problem solutions.

case	Δ_r [%]	Δ_m [μV/m]	T_{op} [K]
1	1.5	9	6
2	0.9	10	21
3	2.8	9	21
4	5	11	21
5	5.6	75	21
6	0.4	4	32
7	2.6	9	32
8	−0.7	5	48
9	−1.9	6	50
10	2.4	4	70

to a maximum current at which the magnet could be operated for long time at constant operation current. With such measurement, the parameters related to the heat generation could be found and the constant operation current phase would give information on the balance between heat generation and cooling, making it possible to find a solution for the cooling coefficient.

5.3. Predictiveness of the thermal model

Next we study, how well the thermal model is able to predict the magnet behavior in various different operation conditions. This is done by fixing the model with parameter values corresponding to the best solution. Hence, we chose the parameter values of the solution $\mathbf{x}_6$ and utilized the model M to test if it was able to predict the thermal behavior of Feather-M2 in all of the investigated cases. The solution was obtained using the data measured at 32 K operation temperature. The results are shown in figure 7 and table 8.

According to the results, it can be noticed that the model is not able to describe the magnet behavior in the whole range of operation temperatures (5-70 K). Relatively good predictions are obtained in the cases where the operation temperature is 21-32 K. Clearly, the linear cooling model (10) does not work well

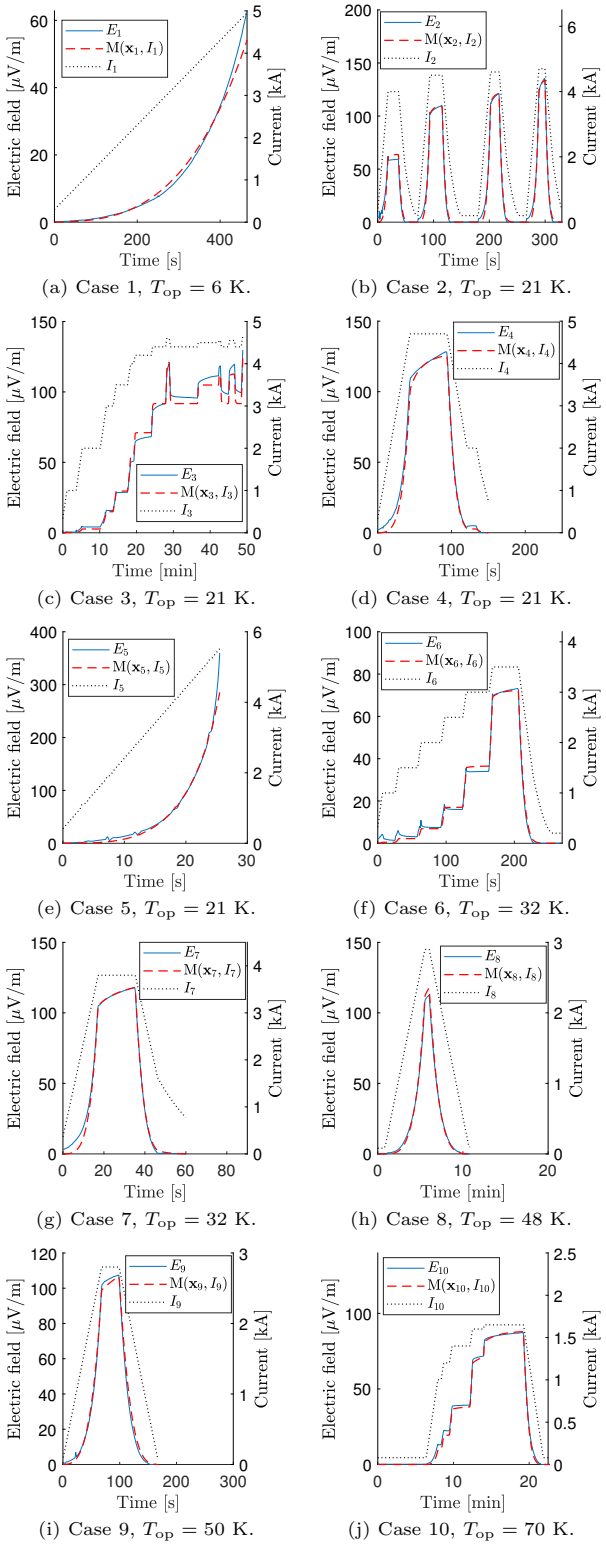

(a) Case 1, T_{op} = 6 K. (b) Case 2, T_{op} = 21 K.
(c) Case 3, T_{op} = 21 K. (d) Case 4, T_{op} = 21 K.
(e) Case 5, T_{op} = 21 K. (f) Case 6, T_{op} = 32 K.
(g) Case 7, T_{op} = 32 K. (h) Case 8, T_{op} = 48 K.
(i) Case 9, T_{op} = 50 K. (j) Case 10, T_{op} = 70 K.

Figure 6. Figures (a)-(j) represent, in each case $i = 1...10$, the measured and simulated average electric field E_i as a function of the operation current I_i and time in Feather-M2.

Table 8. Relative and maximum differences of $\mathrm{M}(\mathbf{x}_6)$ in all of the simulation cases. In case 10, the differences could not be computed due to the early thermal runaway.

case	Δ_r [%]	Δ_m [μV/m]	T_op [K]
1	44.0	25	6
2	26.8	36	21
3	22.5	36	21
4	18.7	28	21
5	31.6	158	21
6	0.4	4	32
7	10.5	13	32
8	−81.9	116	48
9	−113.4	144	50
10	—	—	70

if the operation temperature is significantly different compared to the case at which the value was obtained as a solution of an inverse problem. This is especially visible in figure 7 (j) where the model $\mathrm{M}(\mathbf{x}_6)$ predicts the magnet to quench in the case 10 where T_op was 70 K. Moreover, if T_op was higher than in the case 6, the model predicted higher values for electric field than measured. If T_op was lower, than in case 6, the model predicted too low electric field. This indicates too that the cooling model should be more detailed if better correspondence is searched for.

In case 7, the difference was the smallest with differences of $\Delta_\mathrm{r} = 10.5$ and $\Delta_\mathrm{m} = 13$. In both cases, T_op is the same and the model is able to describe magnet's behavior relatively well.

5.4. Prospects and outlook

Next, as an outlook, discussion on the prospects of the developed simulation tool is carried out using an example of one possible use of the simulation tool as follows. Given that, the computational model is parametrized such that it is able to predict $E(I_\mathrm{op})$ behavior of an HTS magnet in some operation conditions. Then, using the simulation tool, investigations could be done on the behavior of the magnet if it was made of cable having higher J_c or steeper $E_\mathrm{sc}(J_\mathrm{sc})$ relation in the sense of n-value. To demonstrate the use of the tool in the described situation, a parametric study for n-value and α was done in case 5 using the inverse problem solution $\mathbf{x}_5$ as the reference values for the parameters.

The average electric field, the maximum temperature in the magnet (T_max), and its time derivative were computed for n-values from 3 to 30 while keeping the other parameter values at $\mathbf{x}_5$. The simulation results of this parametric study are shown in figure 8. As could have been expected, the electric field, shown in figure 8 (a), develops faster with higher values of n. The maximum temperature in the magnet develops relatively fast too as shown in figure 8 (b). This

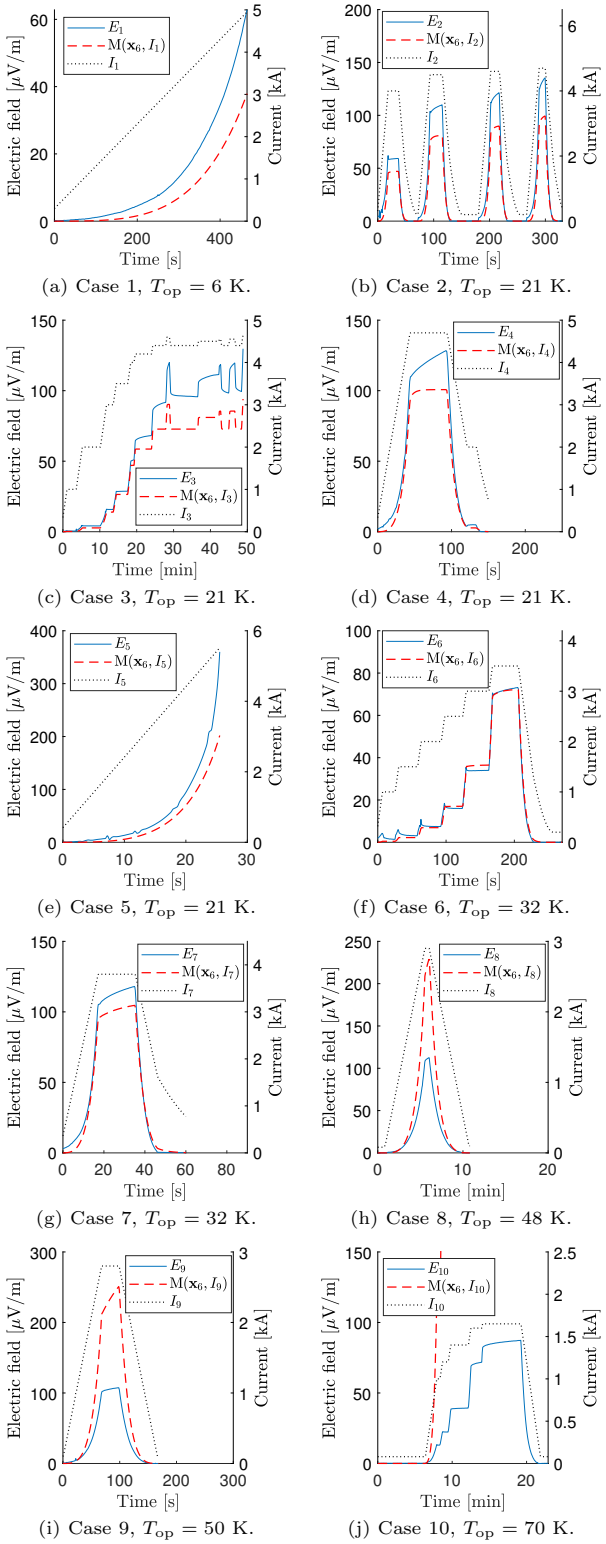

(a) Case 1, $T_\mathrm{op} = 6$ K. (b) Case 2, $T_\mathrm{op} = 21$ K.

(c) Case 3, $T_\mathrm{op} = 21$ K. (d) Case 4, $T_\mathrm{op} = 21$ K.

(e) Case 5, $T_\mathrm{op} = 21$ K. (f) Case 6, $T_\mathrm{op} = 32$ K.

(g) Case 7, $T_\mathrm{op} = 32$ K. (h) Case 8, $T_\mathrm{op} = 48$ K.

(i) Case 9, $T_\mathrm{op} = 50$ K. (j) Case 10, $T_\mathrm{op} = 70$ K.

Figure 7. Figures (a)-(j) represent, in each case $i = 1...10$, the measured and simulated average electric field E_i as a function of the operation current I_i and time in Feather-M2. Simulations were performed using parameter values of the solution $\mathbf{x}_6$.

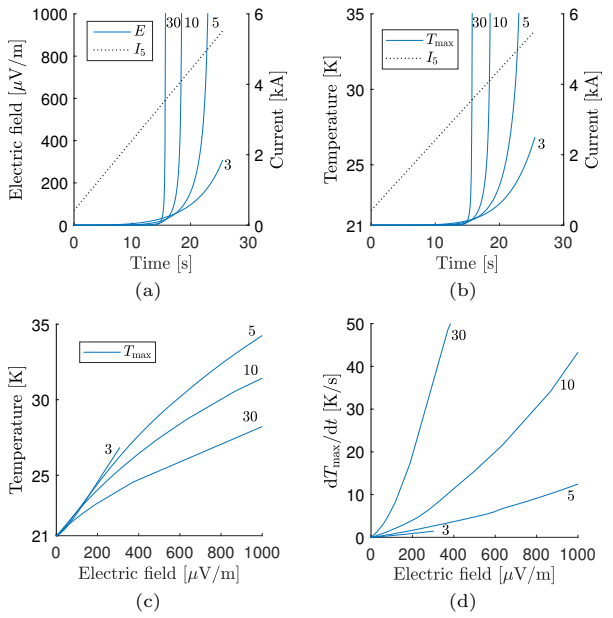

Figure 8. In (a) and (b), the average electric field E and the maximum temperature $T_{\max}$ in the magnet as a function of operation current and time for n-values 3, 5, 10 and 30 is shown, respectively. In (c) and (d), $T_{\max}$ and its time derivative as a function of E is shown, respectively. The other parameters of the model were kept at $\mathbf{x}_5$. The graphs are labeled with the corresponding n-values.

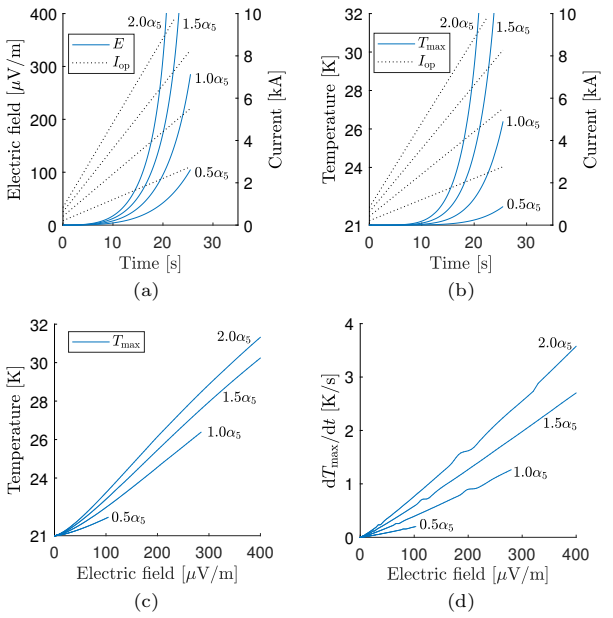

Figure 9. In (a)-(d), the same quantities are shown as in figure 8 for different scale values of the J_c scaling law. The other model parameter values were kept at $\mathbf{x}_5$. The utilized scales were $0.5\alpha_5$, $1.0\alpha_5$, $1.5\alpha_5$ and $2.0\alpha_5$, where $\alpha_5 = 0.15$ as in $\mathbf{x}_5$. The graphs are labeled with the corresponding scales. The operation current I_{op} is obtained by scaling I_5 with 0.5, 1.0, 1.5 and 2.0.

is visible also in figure 8 (c) and figure 8 (d), where $T_{\max}$ and the time derivative of $T_{\max}$ as a function of electric field E are shown, respectively. For example with n-value of 10, at E of 200 μV/m corresponding to $T_{\max}$ of 26.5 K, the time derivative of $T_{\max}$ is already 11 K/s. Based on these results, further investigations on the protectability of the magnet could be done for example.

The scale α of J_c law was varied and the other parameters were kept constant in order to investigate a situation where the magnet was made of different cables each having different critical current density. The utilized J_c scaling law was scaled with $0.5\alpha_5$, $1.0\alpha_5$, $1.5\alpha_5$ and $2.0\alpha_5$, where $\alpha_5 = 0.15$ as in $\mathbf{x}_5$. Respectively, the magnitude of the operation current was scaled with factors 0.5, 1.0, 1.5 and 2.0. The same simulations were performed in this case as done in studying the effects of different n-values. The simulation results are shown in figure 9. The results show that it could be beneficial to have low n-value cable with high electric current carrying capability. Thus, the $T_{\max}$ development would be gradual and the would be more time for protecting the magnet in case of unexpected rising in voltage, as shown in figure 9 (c) and figure 9 (d) where at $E = 400\mu$V/m, corresponding to $T_{\max} = 31$ K, the time derivative of $T_{\max}$ is only 3.5 K/s.

6. Conclusions

In order to study the thermal behavior of an HTS dipole magnet Feather-M2, a thermal model was formulated and parametrized. The parameters were obtained as a solution of inverse problems in 10 cases. These represent various observed magnet behaviors in test cryostat (different operation temperature, operation current and average electric field timeseries). The simulation results show that individual inverse problems could find such model parameters that the corresponding behavior could be very well replicated. The model corresponded to the measured average electric field over the magnet with the average relative and the average maximum absolute difference of 2.4 % and 15 μV/m, respectively, for the ten cases.

When the parameters obtained from one particular inverse problem (32 K and staircase like current ramp for about 4 minutes) were applied to simulate other experimented electric field timeseries, the correspondence between observations and model deteriorated. The smallest error was achieved at the same operation temperature for another current timeseries: the relative error in the average electric field was 10.5 %. At lower temperatures the simulated electric field underestimated the measured electric field whereas at higher temperature it overestimated it. In one case (at 70 K), the model predicted an early thermal runaway that was not observed. Possible reasons, that the

model prediction capability deteriorated for other cases than for which the model parameters were solved for, can be related to the simplified cooling model – or for example to the fact that the helium gas flow rate was not possible to measure during the experiments.

The presented methodology, in which model parameters are solved from an inverse problem, can be utilized in investigating the predictive capability of computational models and their sub-models such as the cooling model in this work. Moreover, the presented simulation tool can be utilized to predict the behavior of a magnet under study in different operation conditions to ensure safe operation.

References

[1] Winkler T and EcoSwing Consortium 2019 *IOP Conf. Ser.: Mater. Sci. Eng.* **502** 012004

[2] van Nugteren J, Kirby G, Murtomaki J, DeRijk G, Rossi L and Stenvall A 2018 *IEEE Transactions on Applied Superconductivity* **28** 4008509

[3] Yanagi N *et al* 2014 *IEEE Transactions on Applied Superconductivity* **24** 4202805

[4] Goldacker W *et al* 2007 *IEEE Transactions on Applied Superconductivity* **17** 3398

[5] Rossi L *et al* 2018 *IEEE Transactions on Applied Superconductivity* **28** 4001810

[6] The European Organization for Nuclear Research, home page: `https://home.cern/`

[7] van Nugteren J *et al* 2018 *Supercond. Sci. Technol.* **31** 065002

[8] van Nugteren J, 2016 *High Temperature Superconducting Accelerator Magnets*. Doctoral thesis, University of Twente, Twente, Netherlands

[9] Härö E *et al* 2013 *IEEE Trans. Appl. Supercond.* **23** 4600104

[10] Ruuskanen J, Stenvall A and Lahtinen V 2017 *IEEE Transactions on Applied Superconductivity* **27** 0600205

[11] Breschi M, Cavallucci L, Ribani P L, Gavrilin A V and Weijers H W 2016 *Supercond. Sci. Technol.* **29** 055002

[12] Markiewicz W Denis, Jaroszynski J, Abraimov D, Joyner R and Khan A 2015 *Supercond. Sci. Technol.* **29** 025001

[13] Hahn S, Park D, Bascunan J and Iwasa Y 2011 *IEEE Transactions on Applied Superconductivity* **21** 1592

[14] Lehtonen J, Mikkonen R and Paasi J 1998 *Physica C* **310** 340

[15] Ishiyama A and Asai H 2001 *IEEE Transactions on Appiled Superconductivity* **11** 1832

[16] Vysotsky V S, Rakhmanov A L and Ilyin Yu A, "Novel approaches to describe stability and quench of HTS devices," in Superconductivity Research Developments. Commack, NY, USA: Nova, 2008, ch. 9.

[17] Rostila L *et al* 2007 *Supercond. Sci. Technol.* **20** 1097

[18] Nättilä J, "X-ray bursts as a tool to constrain the equation of state of the ultra-dense matter inside neutron stars". Doctoral thesis, University of Turku (2017). Available online at `http://urn.fi/URN:ISBN:978-951-29-7057-5`.

[19] van Nugteren J *et al* 2018 *IEEE Transactions on Applied Superconductivity* **28** 4901505

[20] Ruuskanen J, Stenvall A, Lahtinen V, van Nugteren J, Kirby G and Murtomaki J 2019 *IEEE Transactions on Applied Superconductivity* **29** 4701204

[21] `http://www.superox.ru/en/`

[22] `http://i-sunam.com/`

[23] Chambrillon J et al 2011 CERN SRF assembling and test facilities Proc. SRF11 (Chicago) vol 5, pp 530-2

[24] Stenvall A, Korpela A, Mikkonen R and Grasso G 2006 *Supercond. Sci. Technol.* **19** 184

[25] MATLAB, The MathWorks, Inc., Natick, Massachusetts, United States.

[26] Stenvall A, Platform for programming finite element method solvers in Matlab. `https://github.com/stenvala/dp`

[27] van Nugteren J, "Internship Report: CERN, Software development for the Science and Design behind Superconducting Magnet Systems," tech. rep., Uni- versity of Twente: Energy Materials and Systems and CERN: ATLAS magnet team, 2011

[28] Hosea ME and Shampine LF 1996 *Applied Numerical Mathematics* **20** 21

[29] Byrd R, Gilbert J and Nocedal J 2000 *Math. Program.* **89** 149

[30] Fujikura Europe Ltd, 2G YBCO High Temperature Superconductors. Website: `https://www.fujikura.co.uk/`

[31] Murtomaki J, van Nugteren J, Kirby G, Rossi L, Ruuskanen J and Stenvall A 2017 *IEEE Transactions on Applied Superconductivity* **27** 4100405

[32] Edelman H S and Larbalestier D C 1993 *Journal of Applied Physics* **74** 3312-3315

[33] Manfreda G, "Review of ROXIE's Material Properties Database for Quench Simulation", CERN Internal Note 2011-24, EDMS 1178007.

[34] Lu J, Choi E S and Zhou H D 2008 *Journal of Applied Physics* **103** 064908

[35] Smith DR and Fickett FR 1995 *Journal of Research of the National Institute of Standards and Technology* **100** 119

[36] Naito T *et al* 2010 *Supercond. Sci. Technol.* **23** 105013